



ORIGINAL ARTICLE

Efficient loading and delivery of ciprofloxacin by smart alginate/carboxylated graphene oxide/aminated chitosan composite microbeads: *In vitro* release and kinetic studies



Abdelazeem S. Eltaweil^{a,*}, Maha S. Ahmed^a, Gehan M. El-Subruiti^a,
Randa E. Khalifa^b, Ahmed M. Omer^{b,*}

^a Chemistry Department, Faculty of Science, Alexandria University, Alexandria, Egypt

^b Polymer Materials Research Department, Advanced Technology and New Materials Research Institute (ATNMRI), City of Scientific Research and Technological Applications (SRTA-City), New Borg El-Arab City, P. O. Box: 21934, Alexandria, Egypt

Received 20 October 2022; accepted 31 December 2022

Available online 5 January 2023

KEYWORDS

Carboxylated graphene oxide;
Aminated chitosan;
pH-sensitive;
Ciprofloxacin release;
Kinetics

Abstract New composite microbeads were formulated as smart pH-sensitive vehicle for efficient delivery of ciprofloxacin (CIP) drug. Herein, carboxylated graphene oxide (CGO) was successfully impregnated into alginate (Alg) microbeads, which were then coated with aminated chitosan (AmCs) layer to form core-shell Alg/CGO@AmCs composite microbeads. Diverse analysis tools comprising FTIR, TGA, XRD and SEM were employed to characterize the developed carriers, while their swelling profiles and pH-sensitivity were examined under different pHs. The results clarified that increasing CGO and AmCs concentrations in microbeads matrix greatly protected Alg microbeads from fast disintegration at colon pH and prolonged their swelling time. Moreover, about 94.65 % of CIP drug was successfully loaded by Alg/CGO@AmCs composite microbeads compared to 61.95 % for Alg microbeads, confirming their reduced porosity. The *in vitro* CIP-release profiles were investigated in simulated gastrointestinal conditions. Furthermore, increasing AmCs concentration in the outer shell of composite microbeads clearly minimized the CIP burst release at the colon region and offered a sustained release performance. Besides, the CIP release mechanism was well-described by korsmeyer-peppas kinetic model. The cytotoxicity study confirmed the potential safety of the Alg/CGO@AmCs composite microbeads with human cell viability

* Corresponding authors.

E-mail addresses: abdelazeemeltaweil@alexu.edu.eg (A.S. Eltaweil), amomar@srtacity.sci.eg (A.M. Omer).

Peer review under responsibility of King Saud University.



reached 98.98 %, suggesting their applicability as smart carriers for oral delivery of antibiotics.

© 2023 The Author(s). Published by Elsevier B.V. on behalf of King Saud University. This is an open access article under the CC BY-NC-ND license (<http://creativecommons.org/licenses/by-nc-nd/4.0/>).

1. Introduction

Drug delivery technology is a cutting-edge field of science that employs a multidisciplinary scientific approach to improve human health care (Maiti and Sen, 2017). Drug delivery systems (DDSs) that use a variety of carriers such as soluble polymers, dendrimers, microspheres, hydrogel, graphene quantum dots, graphene oxide and emulsions have been developed to overcome the limitations of traditional therapeutics (Lengyel et al., 2019; Liu et al., 2018). Compared to traditional dosage forms, DDSs display a number of benefits, including improved efficacy, reduced toxicity and improved patient compliance and convenience (Li et al., 2019). On contrary, the DDS drawbacks are represented by poor water solubility, aggregation, lack of selectivity toward cancerous cells and non-specific/nano-local biodistribution. In addition to systematic toxicity, low therapeutic index, high drug dose, multidrug resistance, physiological degradation, low circulation half-life and repeated administration (Dikmen et al., 2011; Adepu and Ramakrishna, 2021). A great effort is still needed to vanquish the drawbacks of the DDS and obtain a more effective drug carrier design. The oral route is still considered the most attractive method for drug delivery (Homayun et al., 2019). Specifically, it has the potential to provide solid formulations with a long shelf life, sustained delivery, simplicity of administration and a stronger immunological response (Zhang et al., 2020). Although, for some medications, the oral route also has a number of shortcomings, since the drugs-based oral carriers are broken down and disintegrated by the extremely acidic medium of the stomach and by enzymatic action in the upper small intestinal tract (Tahtat et al., 2013; Deshayes et al., 2021). Thus, the development of pH-responsive biopolymeric carriers such as alginate and chitosan for oral delivery has sparked a lot of interest over the last twenty years (Sung and Kim, 2020; Omer et al., 2021a).

Alginate is a water-soluble linear polysaccharide consists of alternating blocks of 1–4 linked α -L-guluronic and β -D-mannuronic acid residues and can be extracted from natural brown seaweeds (Eltaweil et al., 2022a, Taher et al., 2019). Whereas, chitosan is composed of randomly positioned N-acetyl glucosamine groups and 1–4 connected D-glucosamine residues and can be extracted from the exoskeleton of crabs, shrimps and lobsters the (Eltaweil et al., 2022b; Ding and Guo, 2022; Mohy Eldin et al., 2017). Owing to their outstanding properties comprising their natural abundance, excellent biodegradability, biocompatibility, non-antigenicity, non-toxicity and bio-adhesive property, alginate and chitosan biopolymers have been extensively used in abundant biomedical purposes such as drug delivery, tissue engineering and wound dressing (Li et al., 2022; Kibungu et al., 2021). Therefore, their bio adhesive properties potentially permit a prolonged interaction of the delivered drug, which may improve its absorption efficiency. Both of alginate and chitosan are polyelectrolytes and demonstrate pH-sensitive character involving the protonation of NH_2 groups of chitosan at low

pHs and deprotonation of COOH groups of alginate at high pHs (Omer et al., 2021b; Ghorbani et al., 2015). This pH-sensitivity can be exploited to customize the drug release profiles. Accordingly, alginate and chitosan have been extensively used as smart pH-sensitive vehicles for delivering various drugs through gastrointestinal tract (GI) (Mohy Eldin et al., 2015; Li et al., 2022). Nevertheless, the high porosity of alginate microcapsules produces drug leakage through the formulation process as well as their instability at colon site leads to the drug-burst release (Rafi and Mahkam, 2015). In addition, the poor solubility of chitosan in water and ease of solubility in acidic medium limits its aptitude for controlling the release of encapsulated drugs (Du et al., 2015). To overcome these drawbacks, various physicochemical modifications have employed such as grafting (Mohy Eldin et al., 2015), layered-coating (Sun et al., 2019a), crosslinking (Ubaid and Murtaza, 2018) and composite formation with metal oxide, carbon nanotubes and graphene oxide (Sengupta et al., 2021; Pooresmaeil et al., 2021).

Graphene oxide (GO) has a two-dimensional (2D) honeycomb lattice structure with oxygen functional groups (e.g., OH and COOH) attached to the basal planes and edges of GO sheets (Kim et al., 2012). These active functional groups provide excellent ability to immobilize a large number of substances including metals, drugs, biomolecules, and fluorescent molecules through π -conjugated structure formation (Attia et al., 2021, Basha et al.). In addition, GO has made far-reaching developments in many different industrial, water treatment and biomedical fields owing its excellent characteristics such as biocompatibility, pH sensitivity, higher surface area, excellent mechanical strength, and relatively easy and cost-effective synthesis techniques (Omer et al., 2022; Liu et al., 2018; Khan et al., 2021). Thus, naturally functionalized GO by alginate or chitosan is an appropriate candidate for being employed as smart carriers for targeted drug/ gene delivery, antitumor drug delivery, controlled and stimuli-responsive release of various drugs (Olate-Moya and Palza, 2022).

Taking advantage of alginate and chitosan biopolymers as well as the appealing characteristics of GO, an attempt was made in this study to construct efficient pH-responsive core-shell Alg/CGO@AmCs composite microbeads for efficient loading and release of Ciprofloxacin (CIP; antibiotic drug) at colon-site. Herein, GO was firstly functionalized with extra COOH groups (CGO) followed with impregnation into alginate microbeads to lessen their porosity, boost hydrophilicity and improve their stability at colon conditions. Next, the formulated Alg/CGO composite microbeads were further coated with aminated chitosan layer (AmCs) that developed with extra additional amine groups to get core-shell composite microbeads, which are expected to ameliorate the pH-sensitivity of composite microbeads at GI-tract, prevent the drug leaching and provides a sustained drug release manner. The as-constructed composite microbeads were characterized using various analysis tools. Impacts of variation of CGO and AmCs concentrations on the CIP loading efficiency were investigated. Moreover, pH-sensitivity of the developed smart

composite microbeads was investigated through studying their swelling and *in vitro* CIP release profiles under simulated GI-tract conditions. Furthermore, various kinetics models were preformed to identify the release mechanism of CIP, while cellular toxicity study was also examined using Wi38 cells.

2. Experimental

2.1. Materials

Chitin from shrimp shells (Acetylated > 95%), Graphite powder (purity 98%), sodium alginate (SA; Mw = 1.93×10^5 g/mol, M/G = 1.51, viscosity = 200 ± 20 mPa. s), Ciprofloxacin (CIP; assay $\geq 98\%$), Para-benzoquinone (PBQ; assay $\geq 94\%$) and Ethylenediamine (EDA; assay $\geq 99\%$) were purchased from Sigma–Aldrich Chemicals Ltd (Germany). Calcium chloride dehydrate (assay 98%) and Chloroacetic acid (assay 99%) were acquired by Loba Chemie Ltd (India). Acetic acid (assay 99.8%), Sodium hydroxide (pellets; assay 98%), Hydrochloric acid (assay 37%), Dimethyl sulfoxide (DMSO; assay 99%) and Ethanol (assay 99%) were delivered by El-Nasr Pharmaceutical Co. (Egypt).

2.2. Synthesis of AmCs derivative

Aminated chitosan (AmCs) derivative was synthesized following the authors' previous work as depicted in Fig. 1(i) (Omer et al., 2021c). In brief, an exact amount of chitin (8 g) was dispersed under gentle stirring in PBQ (6.9 mM; pH 10) solution for activation of OH⁻ groups of chitin. The reaction mixture was conducted for 6 h at 30 °C. Next, the activated chitin was separated and washed many times by distilled water to eliminate the unreacted PBQ molecules. For the amination step, activated chitin was immersed in EDA (1.8 mM;) solution at room temperature for further 6 h. Subsequently, the produced aminated chitin separated and washed several times by distilled water to eliminate the residual EDA molecules. Finally, the produced aminated chitin was deacetylated using NaOH (50%) for 12 h; 120 °C. The resultant aminated chitosan was separated by filtration, washed by distilled water until reached neutrality and followed by vacuum drying at 60 °C.

2.3. Synthesis of carboxylated graphene oxide (CGO)

Graphene oxide (GO) was firstly synthesized according to the previously reported Hummer method with a slight modification (Eltaweil et al., 2020). Accurate quantity of the prepared GO (0.25 g) was dispersed into 100 mL of distilled water, followed by addition of 5 g of NaOH and 5 g of ClCH₂COOH. Subsequently, the mixture was sonicated at room temperature for 2 h. The formed carboxylated GO (CGO) was neutralized, washed several times with distilled water/ethanol and finally dried for 12 h at 50 °C.

2.4. Formulation of Alg|CGO@AmCs composite microbeads

The composite microbeads were made utilizing the gelation process with calcium ions as a crosslinking agent (Chen et al., 2022). Alginate was firstly dissolved in hot distilled water

(60 °C) under continuous stirring until complete solubilization. The developed CGO was then dispersed in distilled water and slowly added into Alg solution. The final concentration of CGO was 5, 10, and 15%, w/w, while Alg concentration was fixed with a final concentration of 2% w/v. The composite mixture was left under continuous stirring for 1 h at 60 °C before decreasing temperature to 25 °C. Through a fine injection syringe needle (5 cm³), the composite solution was dripped under magnetic stirring into calcium chloride (0.272 mol/L) solution. After curing for 30 min, the resulting spherical wet Alg/CGO composite microbeads were rinsed from the gelling medium and washed several times with distilled to remove the excess of calcium chloride. For core–shell formation, the freshly wet Alg/CGO microbeads were immersed in a solution of aminated chitosan (AmCs; 1, 1.5, and 2%, w/v) as a cationic shell, while pH of coating medium was adjusted at pH 5.5. The coating process was conducted under quite stirring at room temperature for 1 h. Finally, the coated composite microbeads were further intensively washed with distilled water to remove un-coated AmCs followed by drying till reach constant weights. Table 1 displays the compositions concentrations and average diameter of the prepared microbeads; while a schematic diagram describes the formulation process was depicted in Fig. 1(ii).

2.5. CIP-drug loading process

For loading CIP-drug into Alg/CGO@AmCs composite microbeads, an exact quantity of CIP-drug (1 mg/mL) was dissolved in distilled water and subsequently added to the Alg/CGO mixture. Thereafter, CIP-loaded composite microbeads were prepared according to the identical technique as described in section 2.3. The loading efficiency of CIP was determined by soaking a known amount of crushed dried CIP-loaded microbeads in phosphate buffer solution (pH 7.4) for 24 h at 37 °C under shaking conditions (50 rpm), followed by centrifugation. The concentration of loaded CIP was assayed at λ_{max} 277 nm using a UV–vis spectroscopy. The CIP-loading efficiency (%) was calculated according to the following equation (Eq.1) (Khan et al., 2021):

$$\text{CIP – loading efficiency (\%)} = \frac{M_1}{M_0} \times 100 \quad (1)$$

where, M₁ is the quantity of drug in the drug-loaded beads and M₀ represents the initial quantity of CIP-drug.

2.6. Characterization

The chemical structures of the developed composite beads as well as their individual components were verified by Fourier transform infrared spectroscopy (FT-IR, Tensor II, Bruker, Germany). FTIR spectra (4000–500 cm⁻¹) were recorded using 5 mg of dried sample and KBr discs. The morphological properties were clarified using a scanning electron microscope (SEM, Hitachi Limited Ltd, Japan). Prior to SEM analysis, the tested sample was spread on a double-sided conducting adhesive tape pasted on a metallic stub followed by coating with a thin gold film. Furthermore, the crystal structure was investigated by X-ray diffractometer (XRD, BRUKER D8 Advance Cu-K_α radiation, Germany). The XRD generator was operated at 40 kV, 40 mA, and $\lambda = 1.54$ Å. 2-Theta

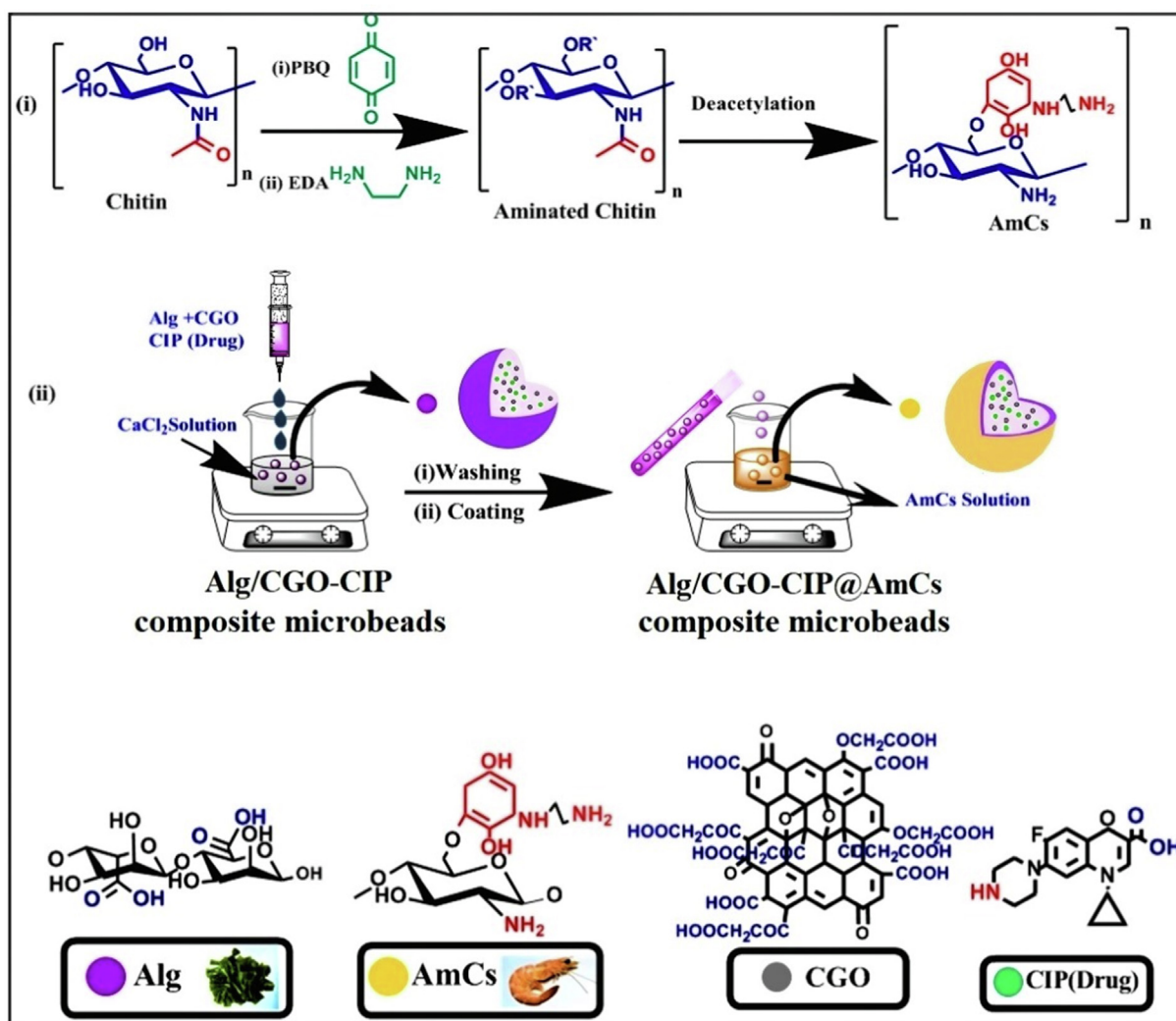


Fig. 1 (i) Proposed scheme the preparation of AmCs and (ii) formulation process of core-shell Alg/CGO@AmCs composite microbeads.

Table 1 Compositions and average diameter of the developed microbeads.

Microbeads code	Compositions	Alg (%)	CGO (%)	AmCs (%)	Average diameter (mm)	
					Wet	Dried
M0	(Alg)	2	—	—	2.83 ± 0.032	0.75 ± 0.021
M1	(Alg/CGO15%)	2	15	—	3.26 ± 0.022	0.84 ± 0.041
M2	(Alg/CGO5%@AmCs1%)	2	5	1	1.92 ± 0.026	0.59 ± 0.033
M3	(Alg/CGO10%@AmCs1%)	2	10	1	2.21 ± 0.028	0.63 ± 0.018
M4	(Alg/CGO15%@AmCs1%)	2	15	1	2.34 ± 0.025	0.67 ± 0.016
M5	(Alg/CGO15%@AmCs1.5%)	2	15	1.5	2.15 ± 0.037	0.61 ± 0.022
M6	(Alg/CGO15%@AmCs2%)	2	15	2	1.87 ± 0.044	0.54 ± 0.025

was started at 10° and was ended at 80°, while the diffraction data was recorded with step of 0.02° and a time of 0.4 s at 25 °C. The thermal properties were examined using Thermo-gravimetric analyzer (TGA, Pyris Diamond TG/DTA,

Perkin-Elmer, USA). TGA curves were performed at a heating rate of 20 °C /min under N₂ atmosphere. Besides, the average size of the formulated microbeads was measured by a digital micrometer screw gauge (Ajanta, India).

2.7. Swelling studies

The swelling profiles of the developed smart pH-sensitive microbeads were investigated using an immersion method (Sun et al., 2019a). A precise weight of examined dried microbeads (0.1 g) was immersed in three different aqueous media: pH 1.2, pH 6.8 and pH 7.4. The swelling experiments were conducted in a shaking water bath (50 rpm) at 37 °C. At time intervals, the swollen microbeads were periodically separated, blotted carefully between two filter papers to remove the excess of the adhered surface water drops and followed by weighing immediately using a closed electronic balance. The percentage of the swelling degree (SD %) was calculated using the following equation:

$$SD (\%) = [(W - W_o) / W_o] \times 100 \quad (2)$$

where, W_o and W are the weights of the dry and swollen sample, respectively.

2.8. In vitro drug release and kinetic studies

The cumulative drug release (CDR) experiments were performed in a shaking water bath (50 rpm) at 37 °C. A definite amount of CIP-loaded microbeads was soaked in separately simulated gastric fluid [SGF; pH 1.2], simulated intestinal fluid (SIF; pH 6.8) and simulated colon fluid (SCF; pH 7.4) using hydrochloric acid and saline phosphate buffers. Approximately, 1 mL of the release medium was taken out at predetermined time intervals, while a fresh medium of the same volume was added to maintain the sink conditions. The cumulative drug release (CDR; %) was estimated via measuring the amount of CIP liberated from the composite microbeads beads at time intervals using a UV-Vis spectrophotometer at 277 nm. The data is presented as the average of at least three separate experiments.

On the other hand, several drug release kinetic models comprising zero-order (Eq. (3)), first-order (Eq. (4)), Higuchi (Eq. (5)) and Korsmeyer - Peppas (Eq. (6)) models were applied to investigate the drug release mechanism according to the following equations (Varma et al., 2004; Kyzioł et al., 2017)

$$Q = k_0 t \quad (3)$$

$$\ln Q = \ln Q_0 - k_1 t \quad (4)$$

$$Q = k_H t^{1/2} \quad (5)$$

$$\ln Q = n \ln t + \ln k_p \quad (6)$$

where, Q is the percentage of the released CIP at time t . k_0 , k_1 , k_p and k_H are the rate constants of the zero-order, first-order, Korsmeyer-Peppas and Higuchi kinetic models, respectively.

2.9. Cytotoxicity study

An *in vitro* cytotoxicity test was performed using an MTT assay (Vinken and Rogiers, 2015). Briefly, 10^5 Wi38 cells were seeded into a 96-well plate and incubated overnight to allow cell attachment. Afterward, the obtained cells were incubated with tested microbeads (31.25–125 µg/mL). The supernatant was separated and poured into an MTT (200 µL, 0.50 mg/mL) solution. After another 4 h, the culture medium was aspi-

rated off followed by addition of DMSO was added to the wells. After eliminating the residual MTT, the cell numbers were estimated and used for the cell cytotoxicity determination.

3. Results and discussion

3.1. Microbeads formulation

Fig. 2 suggests the formation of a complex network with different interactions between the components of microbeads. Alginate biopolymer has the ability to form hydrogels with a three-dimensional network structure in presence of divalent cations such as Ca^{2+} ions. This characteristic permits preparing of drug loaded alginate beads. Therefore, alginate can be transformed into beads using an ionic crosslinking approach. The mechanism of the gelation process includes interactions of guluronic residues (G blocks) of alginate with the specific chelation of Ca^{2+} . Hence, Ca^{2+} ions can ionically coordinate within the cavities produced by a pair of the buckled G sequences creating the so-called “egg-box” structure as the most acceptable theory for describing the formation of calcium alginate microbeads (Borgogna et al., 2013). Further lateral interaction between dimers is mediated by disordered Na^+ and Ca^{2+} cations, H_2O molecules and H-bonding. By incorporation of CGO into Alg microbeads, a single two-dimensional CGO network was combined with a single three-dimensional Alg network (Aparicio-Collado et al., 2022; Choi et al., 2020). The generated extra -COOH groups onto GO sheets promote the interaction between the CGO sheets themselves through Ca^{2+} ions, and strong H-bonding between the CGO sheets and alginate chains. Similarly, the intermolecular H-bonding between AmCs (outer layer) and Alg/CGO took place. Besides, at the optimum pH conditions, the anionic -COO⁻ groups of Alg and CGO can further electrostatically interact with the cationic NH_2 groups of AmCs outer layer, resulting polyelectrolyte complexes (Omer et al., 2021b; Kolanthai et al., 2018; Sun et al., 2019a)).

3.2. FTIR

Fig. 3 shows the FTIR spectra of AmCs, CGO, Alg, Alg/CGO, Alg/CGO@AmCs and Alg/CGO-CIP@AmCs microbeads. The IR spectrum of AmCs showed a broad band at 3437 cm^{-1} which could be attributed to the stretching vibration of $-NH_2$ characteristic groups (Eltaweil et al., 2021). In addition, stretching vibration band for C-H aliphatic was detected at 2990 cm^{-1} , while skeletal vibration at 1076 cm^{-1} is assigned to C-O stretching. The appeared peak at 1656 and 613 cm^{-1} could be ascribed to N-H stretching of the amide group and C-H deformation of β -glycosidic bond, respectively. The spectrum of CGO displayed stretching vibration peaks at 1702, 1043 and 1587 cm^{-1} which assigned to -COOH, C-O and C=C (aromatic rings), respectively (Basha et al., 2022; Meng et al., 2016). Furthermore, IR spectrum of Alg microbeads showed an absorption broad band at 3438 cm^{-1} which corresponds to stretching vibration of OH^- groups (Tamer et al., 2018). This band was shifted after impregnation of CGO into Alg microbeads to the lower wavenumber of 3406 cm^{-1} as shown in Alg/CGO spectrum, proving the successful formulation of composite microbeads.

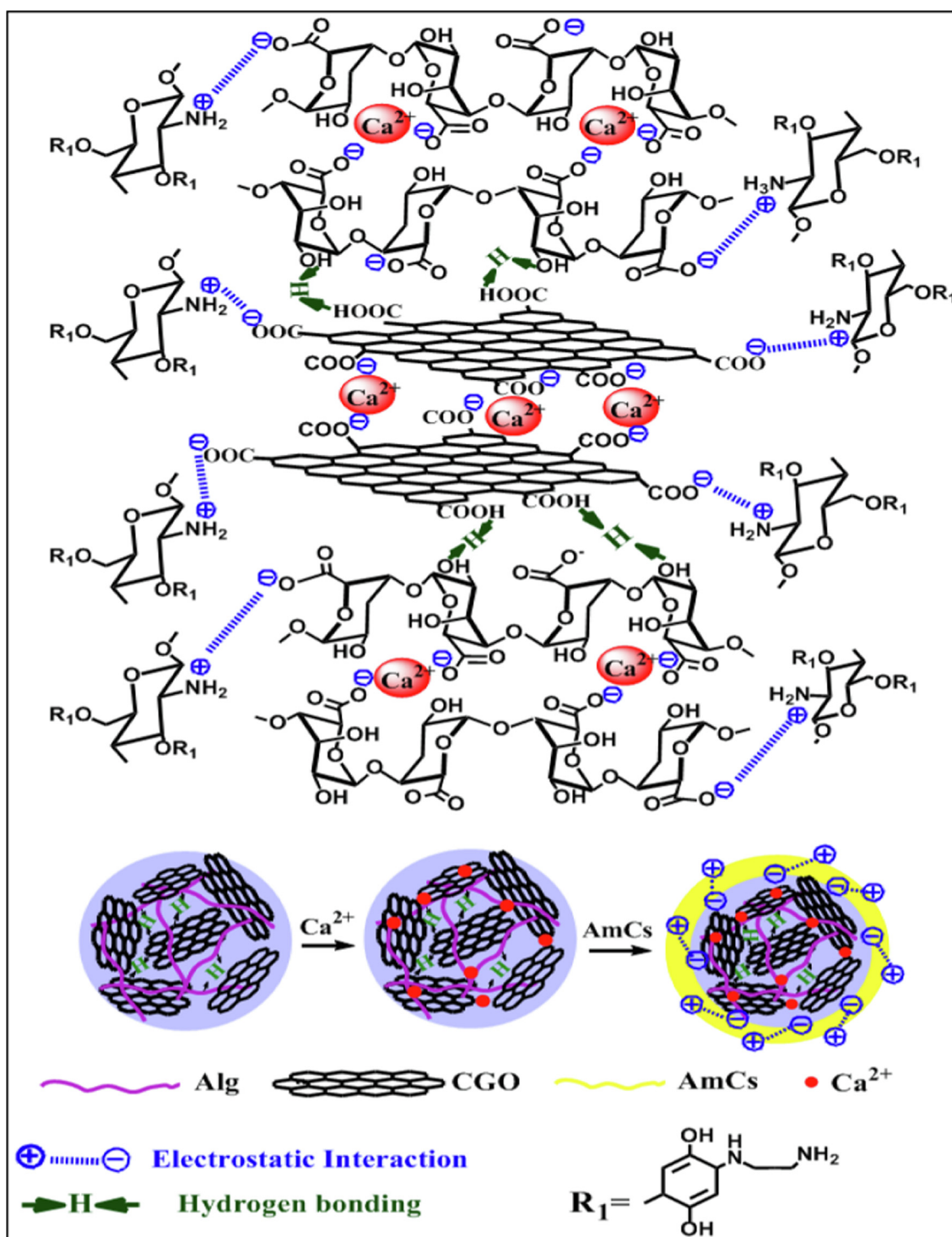


Fig. 2 The possible interactions between functional groups of composite microbeads components.

Also, the characteristic absorption bands at 1627 and 1430 cm^{-1} which were assigned to asymmetric and symmetric -COO stretching vibrations of Alg, (Omer et al., 2021d) were shifted to 1606 and 1424 cm^{-1} as a result of the formation of an interfacial hydrogen bond between CGO and the alginate chain. The peaks at 1035 and 1031 cm^{-1} in Alg and Alg/CGO are referred to skeletal vibration caused by C-O stretching. FTIR spectra reveal the interaction between CGO and Alg

chain. On the other hand, the FTIR spectra of Alg/CGO@AmCs, clarified that the broadening of the band observed at 3436 cm^{-1} may be assigned to the overlapping between NH_2 groups of AmCs and OH groups of CGO and Alg chains. Comparing the spectra of Alg/CGO and Alg/CGO@AmCs, the noticeable shifting from 627 cm^{-1} (in case of Alg/CGO spectrum) to the higher wavenumber of 669 cm^{-1} (in case of Alg/CGO@AmCs spectrum) could be a

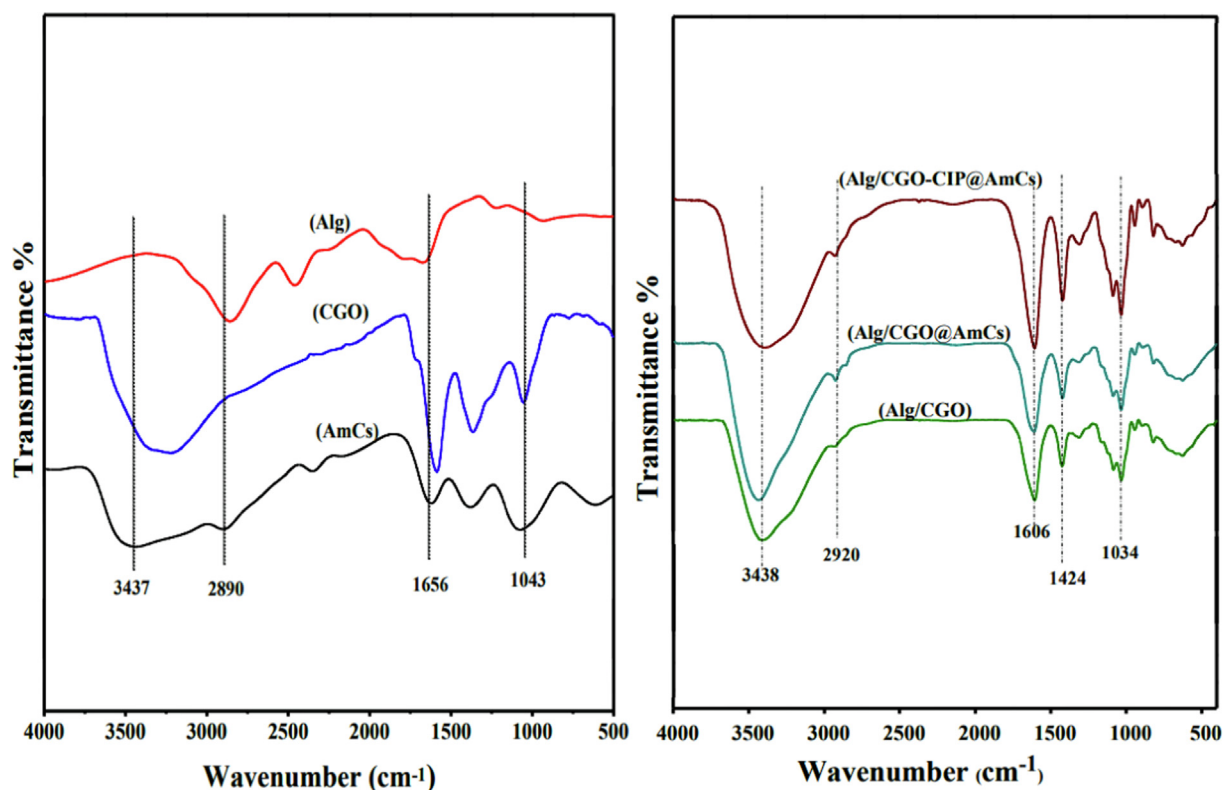


Fig. 3 FTIR spectra of AmCs, CGO, Alg, Alg/CGO, Alg/CGO@AmCs and Alg/CGO-CIP@AmCs composite microbeads.

result of intermolecular hydrogen bonding formation between AmCs (outer layer) and Alg/CGO. Likewise, the characteristic peaks at 1420 and 1309 cm^{-1} represented the C-O stretching vibration and bending vibration of O-H respectively, which indicated the presence of carboxylic groups (Rehman et al., 2021). Besides, the strong absorption peak at 1606 cm^{-1} that exists in the Alg/CGO-CIP@AmCs spectrum could be related to the stretching vibration of the phenyl framework conjugated to -COOH in CIP drug structure. The detected shift from 3436 to 3398 cm^{-1} indicated that basic CIP sites interact strongly with impregnated CGO (Sahoo et al., 2011).

3.3. XRD

The XRD patterns clarified that AmCs (Fig. 4a) exhibited the basic characteristic peaks at 2θ values of 19.67°, 10.33° and 22.31° due to the regularity of the AmCs chain. In the XRD pattern of CGO, a sharp diffraction peak was observed at $2\theta = 12.09^\circ$ with an interlayer spacing of 0.764 nm, indicating the stacked CGO sheet. In addition, the XRD of the alginate disclosed two weak and broad diffraction peaks at 2θ values of 22.25° and 40.21°, corresponding to a rather amorphous structure. In the pattern of Alg/CGO composite microbeads, the most common peaks in CGO and alginate patterns disappeared, suggesting that the CGO is relatively dispersed and does not aggregate to form an ordered structure through the formulation of Alg/CGO composite microbeads (Sun and Fugetsu, 2013). Besides, the XRD pattern of the Alg/CGO@AmCs displayed diffraction peak intensities at 22.42° and 42.43°, which are higher than those of Alg/CGO as a result of the coating process with the AmCs chains. Accord-

ingly, this led to formation of polyelectrolyte complexes, which positively reflects the crystallinity. The intensity of these peaks decreased in the case of Alg/CGO-CIP@AmCs, indicating that CIP was molecularly dispersed within the polymeric matrix (Zheng et al., 2016).

3.4. TGA

TGA was used to determine the thermal stability of the developed composite microbeads compared to their individual components. Fig. 4b implied that all samples displayed initial weight loss ranged from 11 to 26 % with increasing temperature up to 120 °C due to the evaporation of moisture content, tightly bound water and some organic solvent molecules (Omer et al., 2021e; Tamer et al., 2015). The first degradation stage denotes to the hydrophilicity of the microbeads constituents under the effect of its hydrophilic functional groups such as COOH, OH and NH_2 groups. The second weight loss was observed with increasing temperature beyond 200 °C, resulting from the decomposition process of polysaccharide main chains, in addition to decomposition of the pyranose rings via cleaving of the C-O-C glycosides bonds and disintegration of the substituent groups in the methylated derivatives. On the other hand, the results of CGO thermogram clarified that the thermal decomposition of oxygen-containing functional groups was attained with further increasing temperature up to 387 °C. Furthermore, maximum weigh losses of 60.60, 72.03, 58.46, 59.32, 38.91 and 26.04 % were recorded by AmCs, CGO, Alg, Alg/CGO, Alg/CGO@AmCs and Alg/CGO-CIP@AmCs samples, respectively, with elevating temperature up to 400 °C. The results also demonstrated that ther-

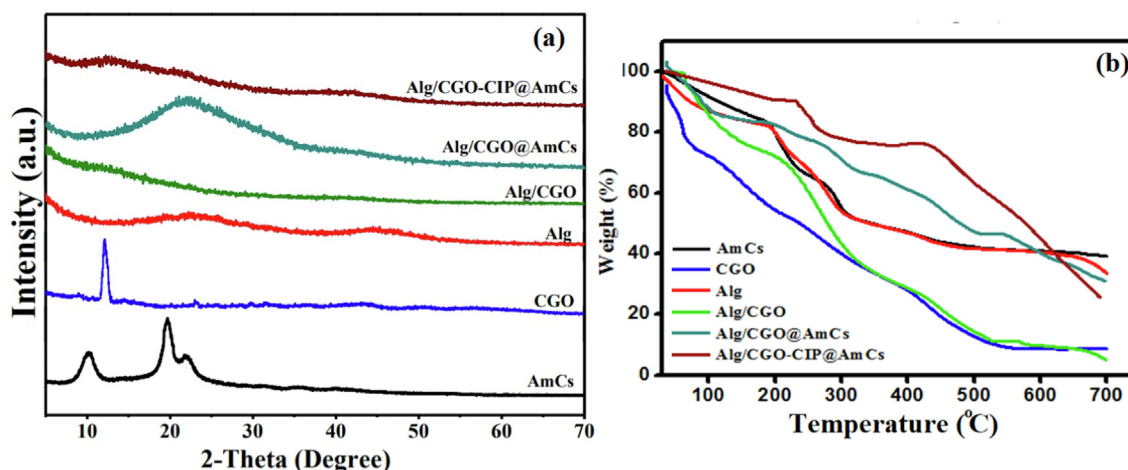


Fig. 4 (a) XRD and (b) TGA curves of AmCs, CGO, Alg, Alg/CGO, Alg/CGO@AmCs and Alg/CGO-CIP@AmCs composite microbeads.

mal stability of alginate microbeads had significantly promoted after incorporation of CGO as well as after coating by AmCs layer. Therefore, the temperature required for Alg/CGO@AmCs microbeads to lose their half weight ($T_{50\%}$ °C) was 478.92 °C compared to 295.49 and 323.17 °C for Alg and Alg/CGO, respectively. These results could be explained by the decent thermal stability nature of graphene oxide and its derivatives, in addition to the hydrogen bonding formation between oxygen-containing groups of the CGO sheet and alginate chains which imparts its thermal stability. Increasing the thermal stability of Alg/CGO beads after coating by AmCs layer could be a result of formation of a strong complexation between the anionic microbeads surface and cationic AmCs coating layer. Besides, the incorporation of the CIP drug into Alg/CGO@AmCs had no significant weight loss up to 240 °C (Chen et al., 2016). However, Alg/CGO-CIP@AmCs microbeads showed better thermal stability compared to drug-free microbeads, since the drug loaded microbeads needed the highest temperature of 523.12 °C to lose 50 % from its initial weight, confirming the acceptable thermal characteristics of the developed drug carrier.

3.5. SEM

The topographical properties of the developed drug carrier were inspected by SEM analysis as shown in Fig. 5. Although the formulated wet microbeads demonstrated smooth and spherical shape, the examined whole surfaces of dried samples were not fully spherical and had rough and irregular shapes as a result of the fast dehydration process during the drying which significantly collapses the hydrogel network (Elnashar et al., 2010). In addition, it was observed that the fracture and whole surface of Alg microbeads (Fig. 5 (a, b)) had intensively affected after the combination with CGO, since it changed from a flat and irregular surface to the rough surface with some cavities (Fig. 5 (c, d)). On the other hand, coating of AmCs on to the developed Alg/CGO composite microbeads clearly changed the morphological surface, as it possessed rougher, denser, fibrillar and rough surface (Fig. 5 (e, f)). The observed change could be attributed to the generated ionic crosslinking through the core-shell formation which might

affect the surface morphology. It was noticed also that the surface morphology of Alg/CGO-CIP@AmCs composite microbeads demonstrated coarser stony surface due to the interfacial interactions of CIP drug through the formation of Alg/CGO-CIP@AmCs composite microbeads (Fig. 5 (g, h)), in addition to the polarity difference between microbeads compositions and drug molecules (Omer et al., 2021a; Sun et al., 2019a).

3.6. Microbeads size measurements

By visual inspection, all freshly prepared wet microbeads were virtually spherical. Table 1 clarified that the average size of wet and dried Alg microbeads was 2.83 ± 0.032 and 0.75 ± 0.021 mm respectively, while it obviously increased after the addition of CGO into Alg microbeads with maximal diameter values reached 3.26 ± 0.022 and 0.84 ± 0.041 mm for wet and dried Alg/CGO microbeads, respectively. At constant 1 % of AmCs, the diameter of coated microbeads was slightly increased from 1.92 ± 0.026 to 2.34 ± 0.025 mm (for wet microbeads) and from 0.59 ± 0.033 to 0.67 ± 0.016 mm (for dried microbeads) with increasing CGO content from 5 to 15 %. On the other hand, the coating process with AmCs layer significantly decreased the diameter due to the shrinkage of the microbeads network in the acidic AmCs medium (Omer et al., 2021b). Therefore, microbeads containing higher AmCs concentration (i.e. 2 %) recorded the minimal size of 1.87 ± 0.044 and 0.54 ± 0.025 mm for wet and dried Alg/CGO15%@AmCs2% microbeads, respectively.

3.7. Swelling and pH sensitivity

The swelling property of smart pH-sensitive drug carriers is an important indicator for the drug release profiles, since it directly affects the controlled and sustained drug release manners. In fact, the swelling process is caused by the hydration of the existing hydrophilic groups (-OH, -COOH and -NH₂) in the microbeads matrix, since the stiff pores inside the hydrogel network are filled by penetrated water molecules from the outer swelling medium, resulting in a larger swelling degree

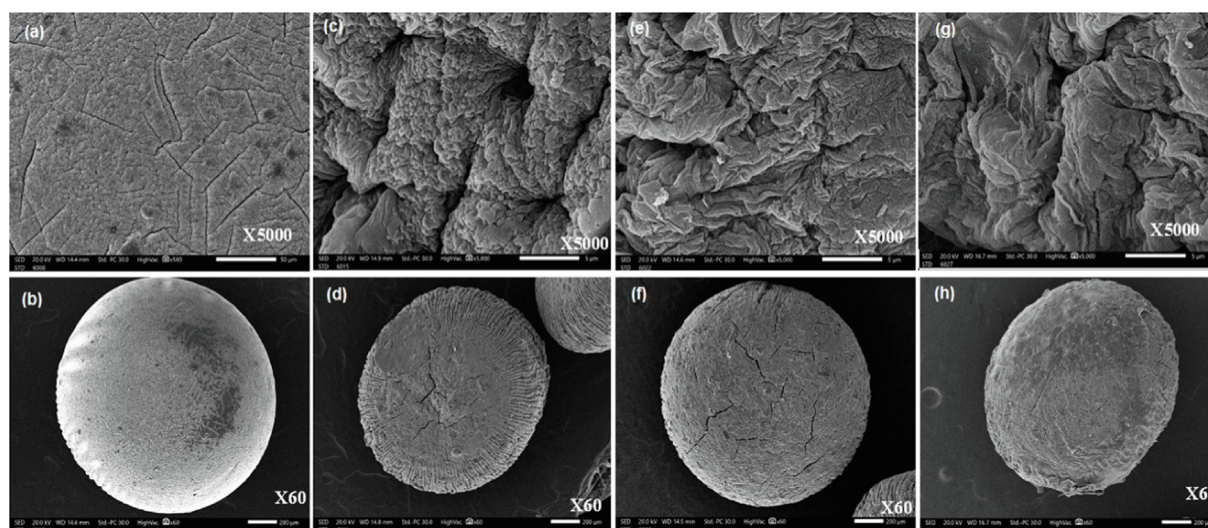


Fig. 5 SEM images for surface and whole microbeads of (a, b) Alg, (c, d) Alg/CGO, (e, f) Alg/CGO@AmCs and (g, h) Alg/CGO-CIP@AmCs composite microbeads at different magnifications.

(SD). Fig. 6a, clarified that Alg microbeads were rapidly swelled with increasing time up to 120 min with a maximal value of 2360 %, followed by disintegration with further increasing the swelling time beyond 120 min. Indeed, fast disintegration of Alg microbeads at high pH could be explained by the higher affinity of Ca^{2+} ions for complexation with the phosphate anions in the swelling medium than alginate matrix, resulting in distortion of microbeads (Omer et al., 2021b; Taher et al., 2019; Sun et al., 2019a). The stability and swelling of Alg microbeads were significantly improved after impregnation of CGO into the microbeads. Therefore, the swelling degree of Alg/CGO composite microbeads was increased gradually from 1738.5 to 2348 % with extending the swelling time up to 210 min due to increasing number of the hydrophilic -OH and -COOH groups, which imparts the hydrophilicity of the composite with microbeads. On the other hand, coating of Alg/CGO microbeads AmCs layer obviously prevented the disintegration of Alg microbeads and, reduced their porosity as well as prolonged the swelling time up to 330 min. However, the core-shell Alg/CGO@AmCs composite microbeads showed a slight decrease in their less swelling degree values compared to Alg and Alg/CGO microbeads due to the existence of AmCs layer on the surface of microbeads, which delayed the swelling rate.

Factually, pH sensitivity of the developed composite microbeads was clearly investigated in three different pH media: pH 7.4, 6.8 and 1.2 under the variation of both CGO and AmCs concentrations. The mechanism of pH sensitivity involves the protonation of NH_2 groups of AmCs shell at acidic conditions and deprotonation of COOH groups of Alg and CGO at high pHs. The results depicted in Fig. 6 (b, d) clarified that increasing the CGO amount embedded in microbeads from 5 to 15 % significantly increased the swelling degree from 1769 to 2312 % and from 1758 to 2163 % at pH 7.4 and pH 6.8, respectively. This could be explained by increasing number of deprotonated -COO^- groups with rising CGO content in composite microbeads, which consequently boost the electrostatic repulsion between the opposite charges, and expands the networks of microbeads, accordingly. In addition,

increasing CGO content create various H-bonds with water molecules, acid groups of alginate chain and hydrophilic groups of other CGO sheets, leading to increasing the swelling degree of Alg/CGO@AmCs composite microbeads (Zhang et al., 2015). On contrary, increasing AmCs concentration from 1 to 2 % resulted in a dramatic decrease in the swelling degree at pH 6.8 (Fig. 6 c) and pH 7.4 (Fig. 6e). This decrease could be attributed to increasing the thickness layer of AmCs on the microbeads surface with increasing AmCs concentration in the coating medium, which hinder the penetration of water molecules into the microbeads network leading to decreasing the swelling degree value.

At low pH 1.2, all studied composite microbeads demonstrated very little swelling degree values compared to those obtained at high pHs (pH 6.8 and 7.4. The hydrated alginate being transformed into a porous and insoluble form (alginic acid skin), since the inter-alginate chains create compact coils which obstruct the swelling of composite microbeads. Besides, a slight increase in the swelling degree was observed with increasing CGO content (Fig. 7a), since more water molecules can interact with the hydrophilic groups in CGO sheet and kept in the microbeads network. The possible reason for this phenomenon might be theoretically correlated with the ionic interactions between the hydrophilic groups of CGO sheets and water molecules. On the other hand, the results signified also that microbeads containing higher concentration of AmCs displayed higher swelling degree value at acidic pH1.2 (Fig. 7b). These observations could be ascribed by increasing number of protonated NH_3^+ groups in the exterior shell of coated microbeads which prompt greater osmotic pressure and improve the intermolecular repulsion leading to increasing the swelling degree (Omer et al., 2021b).

3.8. Evaluation of CIP- loading

An efficient pH-sensitive drug carrier requires high drug loading efficiency to realize the anticipated therapeutic outcome of the drug dose without hampering its action mode. One of the main goals of this research is to improve the CIP-loading effi-

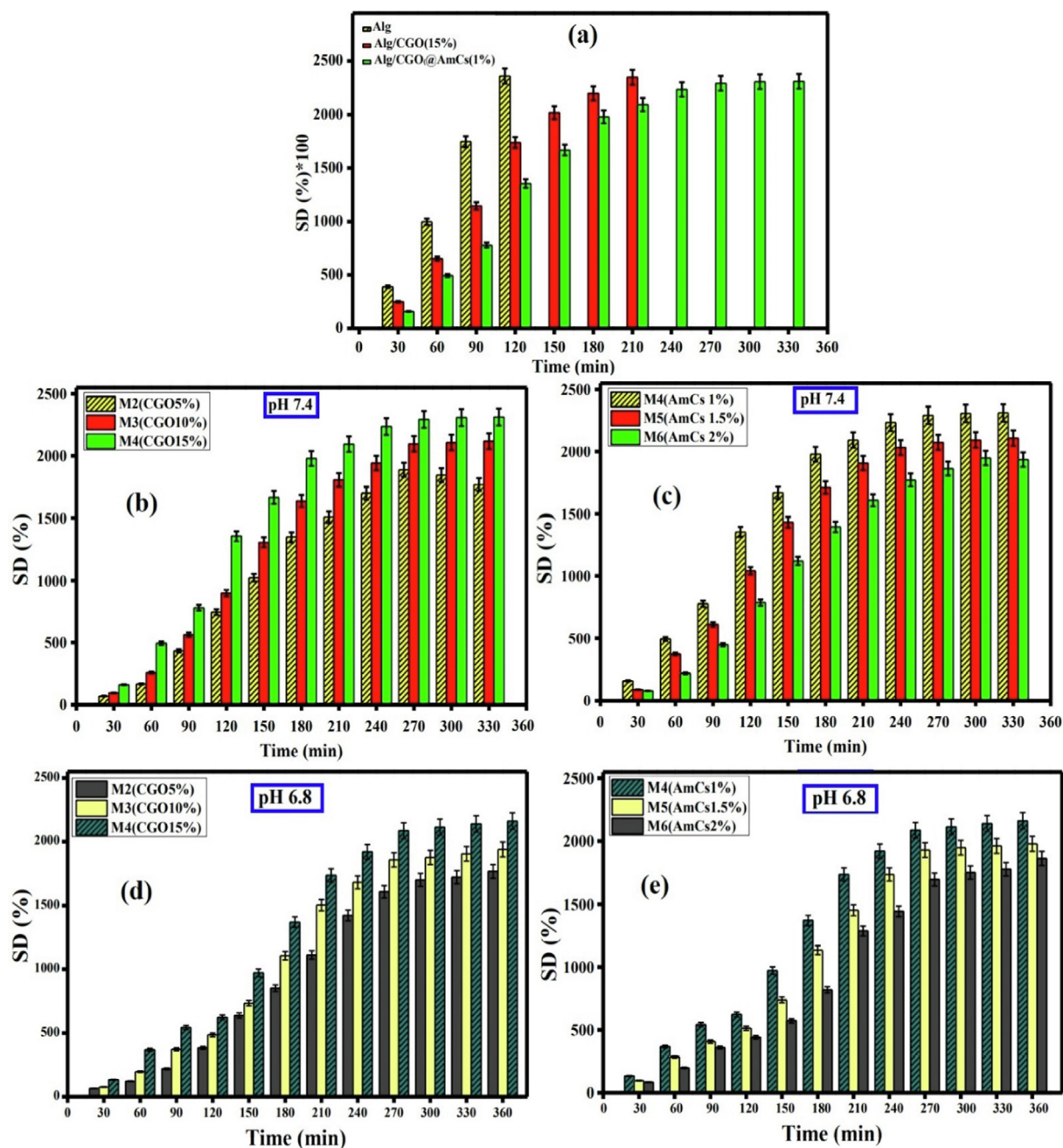


Fig. 6 (a) The swelling degree values of Alg, Alg/CGO and Alg/CGO @ AmCs microbeads at pH 7.4. Effect of (b) CGO amount and (c) AmCs concentration on the swelling degree of microbeads at pH 7.4. Effect of (d) CGO amount (e) AmCs concentration on the swelling degree of microbeads at pH 6.8. All measurements were implemented in triplicates ($n = 3$) and data were presented as mean standard deviation (\pm SD).

ciency of composite microbeads-based alginate through minimizing the amount of medication that is could be leached during the formulation process. The results depicted in Fig. 8a clarified that pure Alg microbeads have the lowest CIP-loading efficiency value of 61.95 % as a result of their higher porosity. A greet improve in the loading efficiency was noticed after the addition of CGO into Alg microbeads, and it gradually increased with rising CGO content up to 15 % with a maximum CIP- loading of 89.08 %. These results could be explained by the probable formation of H-bonding between

the carboxylic groups of CGO and the CIP-NH groups, in addition to π - π stacking interactions, resulting an increase in CIP- loading efficiency. Moreover, the AmCs coated layer had a positive impact on the CIP- loading process, since it prevented the leakage of CIP molecules during the formulation process of core-shell microbeads. Therefore, CIP-loading efficiency was boosted and reached a maximal value of 94.65 % with increasing AmCs concentration in up to 2 % due to increasing viscosity of the coating medium, which might hinder the leakage of CIP molecules from the denser hydrogel matrix

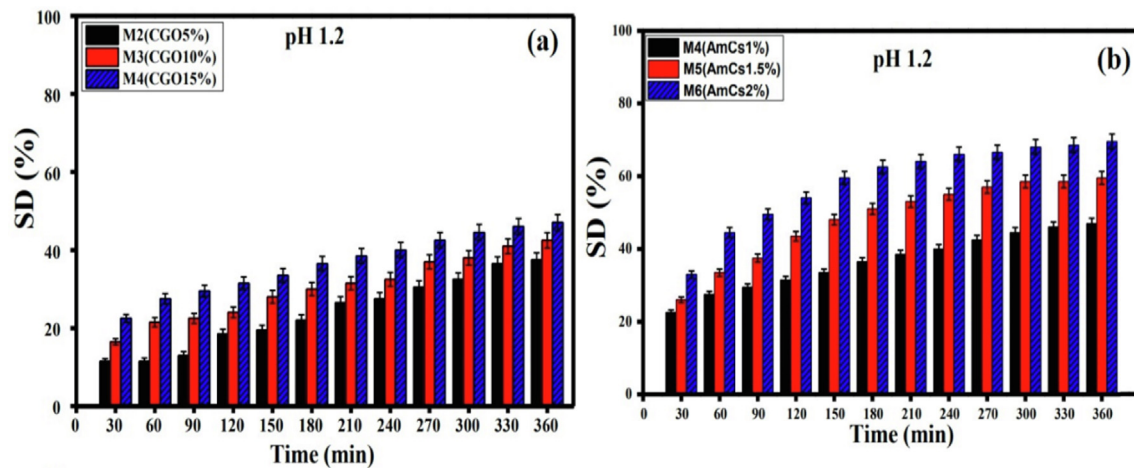


Fig. 7 Effect of (a) CGO amount and (b) AmCs concentration on the swelling degree of microbeads at pH 1.2. All measurements were implemented in triplicates ($n = 3$) and data were presented as mean standard deviation (\pm SD).

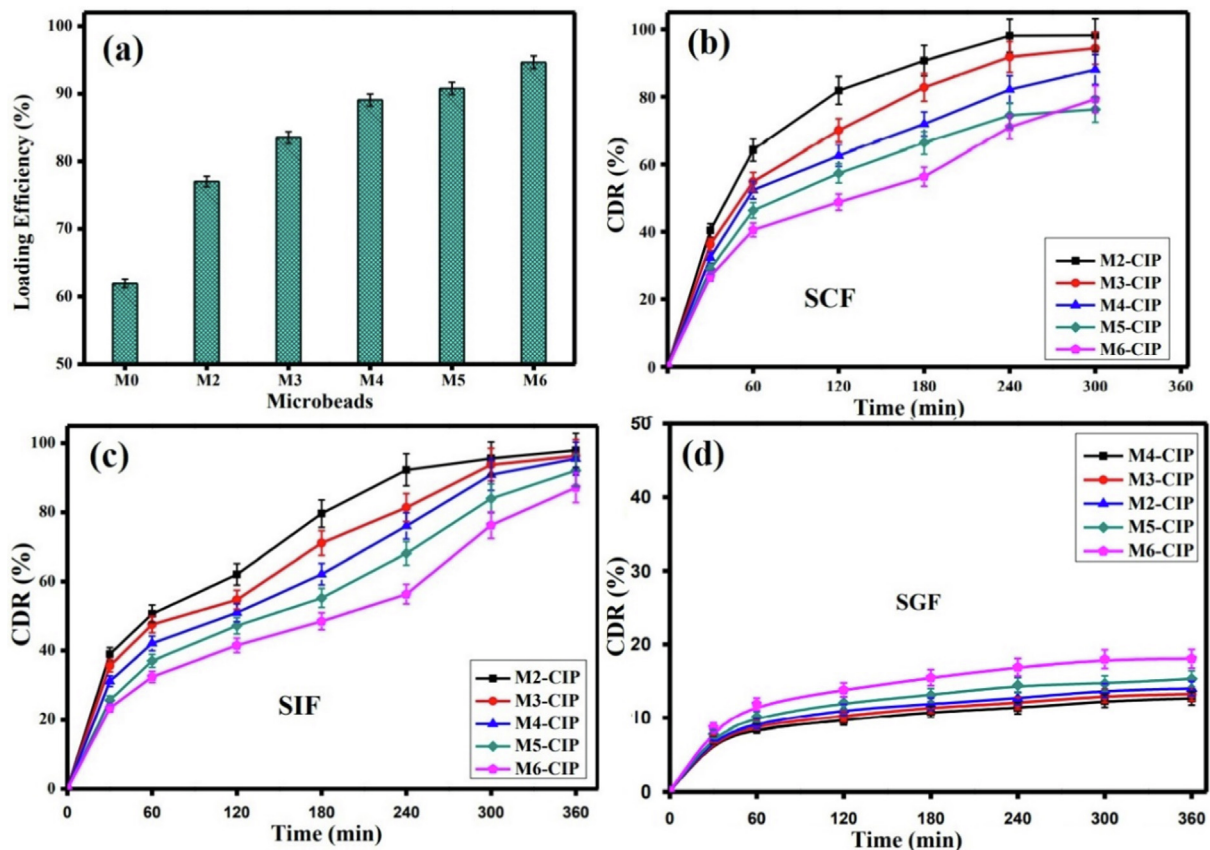


Fig. 8 (a) CIP loading efficiency values. The CDR (%) profiles of Alg-CGO@AmCs composite microbeads at (b) SCF (pH 7.4), (c) SIF (pH 6.8) and (d) SGF (pH 1.2) at 37 °C. All measurements were implemented in triplicates ($n = 3$) and data were presented as mean standard deviation (\pm SD).

(Omer et al., 2021b). As well, the generated electrostatic interactions between negatively charged CIP molecules and the free positively charged NH_2 groups on the microbeads surface resulted in better CIP-loading by the thicker core-shell composite microbeads (Alg/CGO15%@AmCs2%). Table 2 clarified that the developed pH-sensitive Alg/CGO@AmCs composite microbeads showed the highest CIP-loading effi-

ciency value compared to the previously reported CIP-drug carriers, proving the successful loading process.

3.9. *In vitro* CIP release evaluation

The *in vitro* CIP release profiles were investigated in simulated colon (SCF; pH7.4), intestinal (SIF; pH6.8) and gastric (SGF;

Table 2 Comparison of CIP-loading efficiency of Alg-CGO@AmCs composite microbeads with other reported drug delivery systems.

Drug delivery system	CIP-loading efficiency (%)	Ref.
Poly(lactide-co-caprolactone)-PF127 copolymer of Ethylene Oxide/Propylene Oxide microspheres	58–66.6	(Ravindra et al., 2011)
Chitosan-alginate nanoparticles	68.98	(Ghaffari et al., 2012)
Alginate/high methoxyl Pectin/ Guar Gum Alkyl Amine	73.8	(Islan et al., 2015)
Chitosan/alginate beads	74.6	(Kyzioł et al., 2017)
Chitosan beads	75.8	(Srinatha et al., 2008)
Alginate–gelatin blend microspheres	80	(Islan and Castro 2014)
Alg-CGO@AmCs	94.65	This study

pH1.2) conditions. The results clarified that all pH-sensitive Alg-CGO@AmCs composite microbeads demonstrated higher CIP release (%) values at pH 7.4 (Fig. 8b) and pH 6.8 (Fig. 8c) compared to those gained at acidic pH 1.2 (Fig. 8d). In addition, the CIP release from all tested microbeads showed biphasic behavior, i.e., the initial rapid release (burst effect) followed by sustained release manner. In SCF and SIF, the burst CIP release was detected at the early stage (up to 30 min), since CIP was launched from the composite microbeads, while the sustained CIP release period was observed from 30 to 300 min. The impact of the burst release can be explained as adsorbed CIP drug molecules on the surface of the composite

beads during the formulation process. Therefore, migration of CIP drug during the drying step may lead to a heterogeneous distribution of CIP inside microbeads, and followed with burst release. Furthermore, with increasing CGO content, the CIP burst release was reduced and the cumulative drug release (CDR) decreased gradually, which represented a good agreement with the obtained CIP-loading results. Therefore, microbeads contained lower CGO content (i.e. 5 %) recorded maximum CDR of 98.19 and 97.93 % in SCF and SIF, respectively compared to 88.05 % and 95.54 % for microbeads with the highest CGO content (15 %). Decreasing the CIP release (%) values could be a result of possible H-bonding between the carboxylic groups of CGO and -NH groups of CIP drug, in addition to the presence of a strong π - π stacking interaction (Hanna and Saad, 2019). Similarly, increasing AmCs concentration in the composite microbeads up to 2 % clearly minimized the CIP burst release at the initial stage from 40 to 27 % at pH7.4 and from 38 to 23 at pH6.8. Subsequently, a sustained release rate was perceived with minimal CDR values of 79.28 and 87.19 % which were recorded in SCF and SIF with the prolongation of the release time up to 330 and 360 min, respectively. This reveals that the structure of the composite microbeads has been conserved, owing to the existence of AmCs shell, which is partially insoluble at high pHs resulting in a delay in the CIP release rate. The strong charge interactions between ciprofloxacin's carboxylic groups, which were gradually deprotonated at high pH and can bind with the available positively charged AmCs outer shell, resulting in sustained release behavior.

On the contrary, at pH 1.2 [SGF], increasing the amount of CGO didn't show a significant change in the CIP release values, referring to a strong interaction between CIP and composite microbeads. The limited release behavior at acidic conditions could be a reason of (i) the low swelling rate of composite microbeads at pH 1.2; (ii) the stable structure of the Alg/CGO core prevented the microbeads from dissolving;

Table 3 Kinetic models for CIP drug release mechanism.

Microbeads code	Kinetic model	Kinetic model								
		Korsmeyer-Peppas			zero-order		First-order		Huguchi	
		(R ²)	(K) (%/min ⁿ)	(n)*	(R ²)	(K ₀) (%/min ⁻¹)	(R ²)	(K ₁) (min ⁻¹)	(R ²)	(k _H) (%/min ^{0.5})
SCF (pH 7.4)	M2	0.999	4.152	0.6687	0.8837	0.2533	0.7997	0.0037	0.8594	7.213
	M3	0.999	4.707	0.5997	0.9125	0.2077	0.8327	0.0032	0.8973	6.249
	M4	0.9335	6.726	0.4762	0.9279	0.1889	0.8327	0.0032	0.8952	5.659
	M5	0.9552	5.649	0.4930	0.8981	0.1645	0.8071	0.0031	0.8697	5.085
	M6	0.9655	7.143	0.4029	0.9765	0.1833	0.9179	0.0036	0.9658	4.642
	SIF (pH 6.8)	M2	0.9945	12.591	0.3352	0.9335	0.1848	0.8874	0.0027	0.8932
M3		0.9620	12.74	0.3096	0.9753	0.1881	0.9341	0.0029	0.9467	5.5024
M4		0.9907	8.955	0.3703	0.9885	0.1978	0.9551	0.0032	0.9743	5.0732
M5		0.9896	6.2764	0.4220	0.9905	0.1968	0.9492	0.0036	0.9693	4.5618
M6		0.9967	5.8702	0.4104	0.9774	0.1847	0.9675	0.0037	0.9277	4.0648
SGF (pH 1.2)		M2	0.9899	3.241	0.2415	0.9221	0.0172	0.8700	0.0016	0.2343
	M3	0.9934	3.295	0.2485	0.9199	0.0185	0.8678	0.0017	0.1235	0.9526
	M4	0.9956	3.209	0.2332	0.9344	0.0146	0.8858	0.0014	0.3156	0.8294
	M4	0.9956	3.209	0.2332	0.9344	0.0146	0.8858	0.0014	0.3156	0.8294
	M5	0.9872	3.372	0.2607	0.8903	0.0187	0.8250	0.0015	0.0129	1.0017
	M6	0.9748	3.574	0.2794	0.8606	0.0228	0.7911	0.0016	0.1911	1.1672

*Release exponent (n) was evaluated for < 60 % of drug release.

and (iii) CIP had low solubility in the acidic conditions. Nevertheless, a slight increase in CDR (%) values was noticed with increasing AmCs concentration up to 2 % on the surface of composite microbeads. These results could be explained by protonation of NH_2 groups of AmCs at acidic environment, since the electrostatic repulsion increases between the positively charged NH_3^+ groups (Sun et al., 2019b). Thereby, increasing the diffusion coefficient of the CIP molecules within the microbeads matrix and a slight improve in the release pro-

file took place accordingly (Omer et al., 2021b). In all cases, maximum CDR values at SGF were not exceeded 20 % after 360 min.

3.10. Kinetics of CIP drug release

The gained experimental data from CIP drug release investigations at various pHs (pH 7.4, pH 6.8 and pH 1.2) were plotted

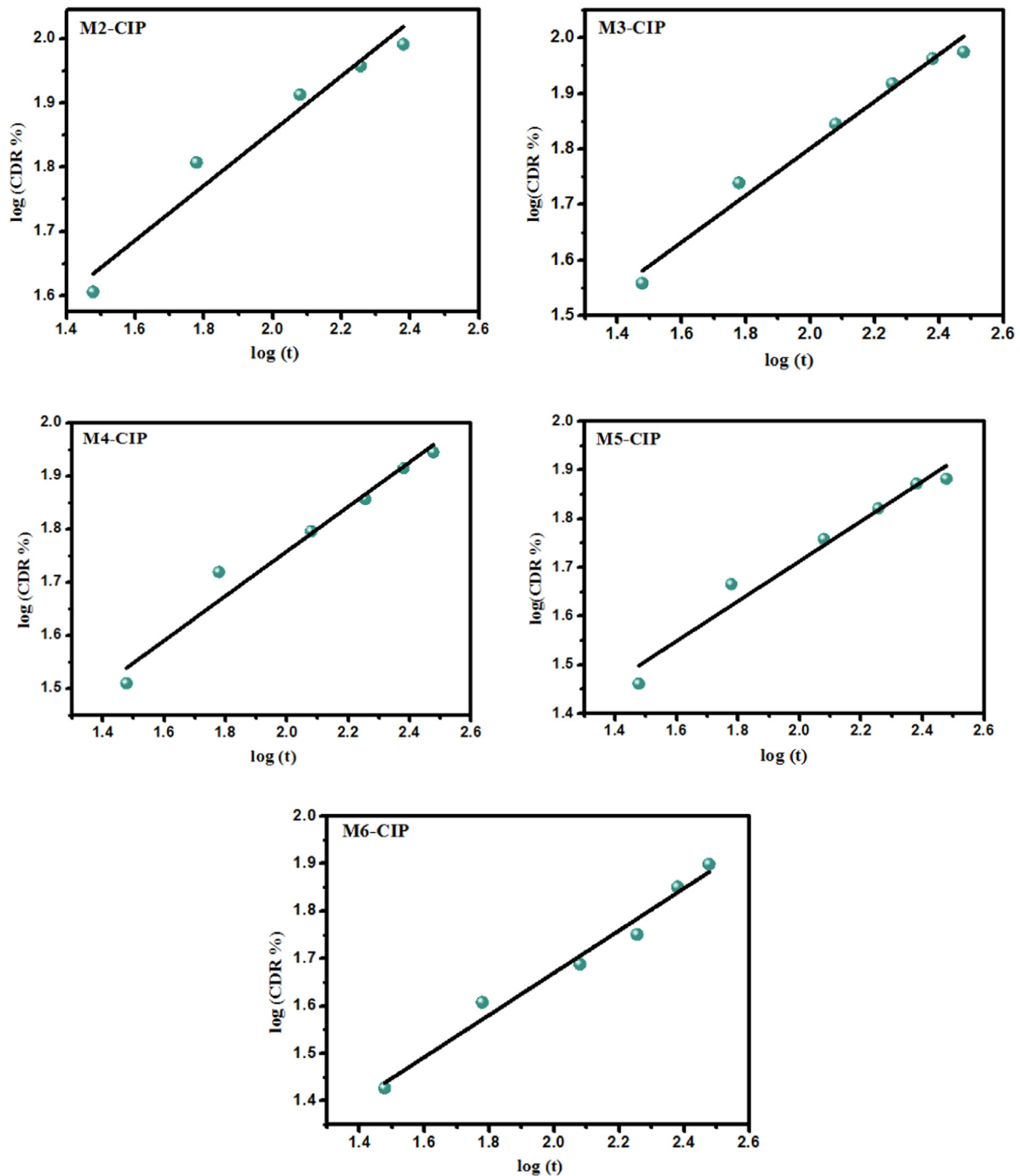
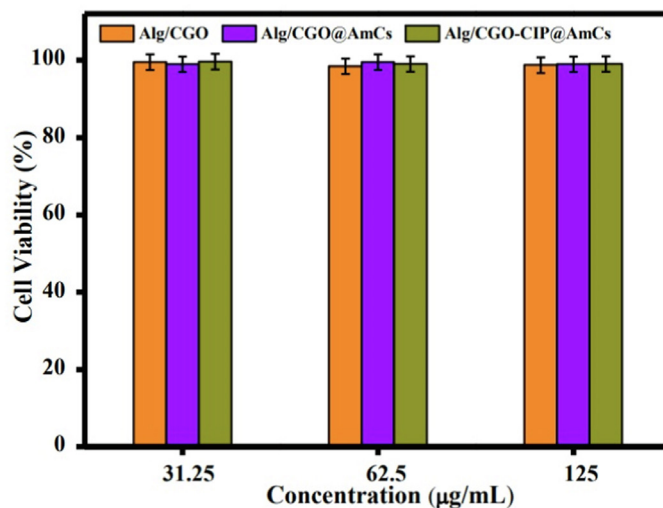


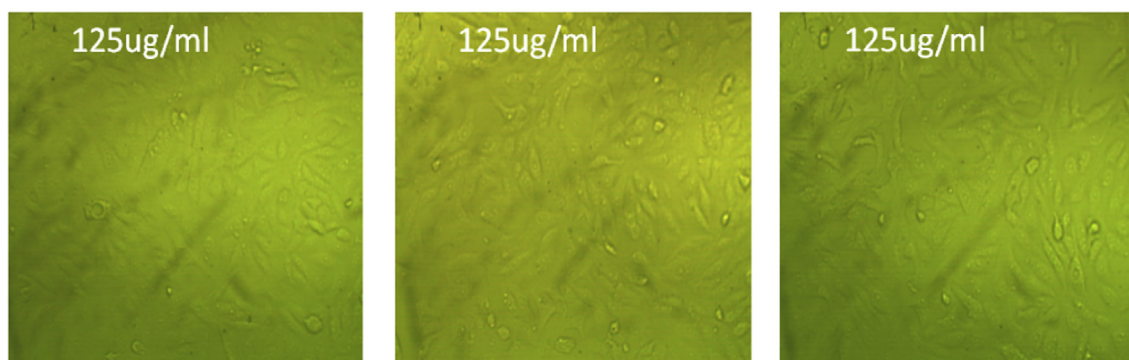
Fig. 9 Mathematical fitting model (Korsmeyer-peppas kinetic model) of the cumulative percentage of CIP release from different composite microbeads at pH 7.4.

in various kinetic models to analyze the release kinetics namely; (i) zero-order, (ii) First-order, (iii) Higuchi mode and (iv) Korsmeyer-Peppas. The correlation coefficients of the release profiles were calculated according to different mathematical models for the analysis of the release kinetics as summarized in Table 3. The mechanism of CIP drug release can be investigated according to Korsmeyer-Peppas by incorporating less than 60 % of release where n is the release exponent, indicative the mechanism of CIP drug release. The results demonstrated that the regression coefficient (R^2) for equation $Q_t = k t^n$ was between 0.96 and 0.99 for most tested microbeads samples, indicating that drug release process followed the Korsmeyer-Peppas kinetic model (Fig. 9). Furthermore, the “ n ” exponent of the Korsmeyer-Peppas model indicates the type of diffusion. The release exponent values were calculated as $n < 0.43$ for spherical microbeads at pH 6.8 and pH 1.2. These results indicated that the CIP release mechanism fol-

lowed the Fickian diffusion law. In addition, when the exponent values ranged between $0.43 < n < 0.83$ (in case of pH 7.4), the CIP drug release rate corresponding to anomalous or non Fickian diffusion. These observations inferred that the drug release mechanism is dependent on both CIP drug diffusion and polymer relaxation. The CIP drug is partially diffused through the swollen network of microbeads matrix (Srinatha et al., 2008; Marei et al., 2019). For instance, at pH 6.8, the zero-order model showed a high R^2 value in M3 and M5 formulations indicated the constant rate of the released CIP drug over a period of time, as the same behavior applied to M6 formulation at pH 7.4. In terms of other medium, the Korsmeyer-Peppas model exhibited superiority over the other models studied for describing the release mechanisms of CIP drug. It takes into account several mechanisms simultaneously, such as diffusion of water into the polymeric microbeads matrix, the swelling and dissolution processes.



(a)



(b)

(c)

(d)

Fig. 10 (a) *In vitro* cell viability assay of Wi38 cell incubated with Alg/CGO, Alg/CGO(15%)@AmCs(1%), and Alg/CGO(15%)-CIP@AmCs(1%) at different concentrations. Optical micrograph of Wi38 treated with (b) Alg/CGO, (c) Alg/CGO@AmCs and (d) Alg/CGO-CIP@AmCs composite microbeads at a concentration of 125 µg/mL.

3.11. Cytotoxicity assessment

The *in vitro* cytotoxicity of the formulated composite microbeads on normal Wi38 cells was investigated by the colorimetric MTT assay. As described in Fig. 10a, no significant toxicity was observed at all studied concentrations (31.25, 62.5 and 125 µg/mL) of tested composite microbeads samples, indicating the potential safety of the developed microbeads toward the normal human cells. The cell viabilities at 125 µg/mL of tested sample were recorded as 98.74 %, 98.98 and 98.82 % for Alg/CGO, Alg/CGO@AmCs and Alg/CGO-CIP@AmCs composite microbeads, respectively. Fig. 10 (b-d) portrayed the optical micrographs of Wi38 cells incubated with the examined composite microbeads at a concentration of 125 µg/mL. It can be observed that number of Wi38 cells decreased but stay active, signifying the lack of observed cytotoxicity of the developed drug carrier (Abdelfattah et al., 2016).

4. Conclusion

Trying to reduce porosity of alginate carriers as well as to maximize their drug encapsulation efficiency, core-shell Alg/CGO@AmCs composite microbeads were developed as pH-sensitive carriers for Ciprofloxacin drug. The developed composite microbeads were investigated their structures, thermal properties, crystallinity and morphological changes using various analysis tools. The results signified that pH-sensitivity and swelling performance of Alg/CGO@AmCs composite microbeads were clearly affected and controlled by the CGO and AmCs concentrations. Maximum CIP-loading efficiency of 94.65 % was achieved by microbeads contained 15 % CGO and coated with 2 % of AmCs, while Alg microbeads recorded only 61.95 %. A sustained release rate was attained with CDR values of 79.28 % at pH7.4 after 330 min, while the best fitted kinetic model for describing the CIP mechanism was korsmeyer-peppas kinetic model. Finally, the developed composite microbeads had no observed toxicity against the human cells, reflecting their safe application as efficient smart carriers for oral delivery and sustained release of drugs.

Funding

This research received no external funding.

Data Availability Statement

The data presented in this study are available on request from the corresponding author.

CRedit authorship contribution statement

Abdelazeem S. Eltaweil: Conceptualization, Formal analysis, Writing – original draft, Writing – review & editing, Supervision. **Maha S. Ahmed:** Methodology, Formal analysis, Writing – original draft. **Gehan M. El-Subruiti:** Writing – review & editing, Supervision. **Randa E. Khalifa:** Formal analysis, Supervision. **Ahmed M. Omer:** Conceptualization, Formal analysis, Writing – original draft, Writing – review & editing, Supervision.

Data Availability Statement

The data presented in this study are available on request from the corresponding author.

Declaration of Competing Interest

The authors declare that they have no known competing financial interests or personal relationships that could have appeared to influence the work reported in this paper.

References

- Abdelfattah, M.I., Nasry, S.A., Mostafa, A.A., 2016. Characterization and cytotoxicity analysis of a ciprofloxacin loaded chitosan/bioglass scaffold on cultured human periodontal ligament stem cells: a preliminary report. Open Access Macedonian J. Med. Sci. 4, 461–467. <https://doi.org/10.3889/oamjms.2016.052>.
- Adepu, S., Ramakrishna, S., 2021. Controlled drug delivery systems: current status and future directions. Molecules 26, 5905–5950. <https://doi.org/10.3390/molecules26195905>.
- Aparicio-Collado, J.L., García-San-Martín, N., Molina-Mateo, J., Torregrosa Cabanilles, C., Donderis Quiles, V., Serrano-Aroca, A., Sabater i Serra, R., 2022. Electroactive calcium-alginate/polycaprolactone/reduced graphene oxide nanohybrid hydrogels for skeletal muscle tissue engineering. Colloids Surf. B Biointerfaces 214. <https://doi.org/10.1016/j.colsurfb.2022.112455> 112455.
- Attia, N.F., Elashery, S.E., Zakria, A.M., Eltaweil, A.S., Oh, H., 2021. Recent advances in graphene sheets as new generation of flame retardant materials. Mater. Sci. Eng. B 274. <https://doi.org/10.1016/j.mseb.2021.115460> 115460.
- Basha, I.K., El-Monaem, A., Eman, M., Khalifa, R.E., Omer, A.M., Eltaweil, A.S., 2022. Sulfonated graphene oxide impregnated cellulose acetate floated beads for adsorption of methylene blue dye: optimization using response surface methodology. Sci. Rep. 12 (1), 9339.
- Borgogna, M., Skjåk-Bræk, G., Paoletti, S., Donati, I., 2013. On the Initial Binding of Alginate by Calcium Ions. The Tilted Egg-Box Hypothesis. J. Phys. Chem. B 117 (24), 7277–7282.
- Chen, G.L., Cai, H.Y., Chen, J.P., Li, R., Zhong, S.Y., Jia, X.J., Liu, X.F., Song, B.B., 2022. Chitosan/Alginate nanoparticles for the enhanced oral antithrombotic activity of clam heparinoid from the clam *Coelomacra antiquata*. Mar. Drugs 20, 136–151. <https://doi.org/10.3390/md20020136>.
- Chen, K., Ling, Y., Cao, C., Li, X., Chen, X., Wang, X., 2016. Chitosan derivatives/reduced graphene oxide/alginate beads for small-molecule drug delivery. Mater. Sci. Eng. C 69, 1222–1228. <https://doi.org/10.1016/j.msec.2016.08.036>.
- Choi, J.W., Kim, H.J., Ryu, H., Oh, S., Choi, S.J., 2020. Three-dimensional double-network hydrogels of graphene oxide, alginate, and polyacrylonitrile for copper removal from aqueous solution. Environ. Eng. Res. 25 (6), 924–929.
- Deshayes, C., Arafath, M.N., Apaïre-Marchais, V., Roger, E., 2021. Drug delivery systems for the oral administration of antimicrobial peptides: promising tools to treat infectious diseases. Front. Med. Technol. 3, 1–13. <https://doi.org/10.3389/fmedt.2021.778645>.
- Dikmen, G., Genç, L., Güney, G., 2011. Advantage and disadvantage in drug delivery systems. J. Mater. Sci. Eng. 5, 468.
- Ding, J., Guo, Y., 2022. Recent advances in chitosan and its derivatives in cancer treatment. Front. Pharmacol. 13, 888740–888753. <https://doi.org/10.3389/fphar.2022.888740>.
- Du, H., Liu, M., Yang, X., Zhai, G., 2015. The design of pH-sensitive chitosan-based formulations for gastrointestinal delivery. Drug Discov. Today 20, 1004–1011. <https://doi.org/10.1016/j.drudis.2015.03.002>.
- Elnashar, M.M., Yassin, M.A., Moneim, A.E.F.A., Bary, E.A., 2010. Investigating the unexpected behavior for the release kinetics of brilliant blue encapsulated into calcium alginate beads. Eurasian Chem. Technol. J. 12, 69–77.
- Eltaweil, A.S., Abd El-Monaem, E.M., Elshishini, H.M., El-Aqapa, H. G., Hosny, M., Abdelfatah, A.M., Ahmed, M.S., Hammad, E.N., El-Subruiti, G.M., Fawzy, M., Omer, A.M., 2022a. Recent

- developments in alginate-based adsorbents for removing phosphate ions from wastewater: a review. *RSC Adv.* 12 (13), 8228–8248.
- Eltaweil, A.S., Hashem, O.A., Abdel-Hamid, H., Abd El-Monaem, E. M., Ayoup, M.S., 2022b. Synthesis of a new magnetic Sulfacetamide-Ethylacetoacetate hydrazone-chitosan Schiff-base for Cr (VI) removal. *Int. J. Biol. Macromol.* 222, 1465–1475.
- Eltaweil, A.S., El-Monaem, E.M.A., Mohy-Eldin, M.S., Omer, A.M., 2021. Fabrication of attapulgite/magnetic aminated chitosan composite as efficient and reusable adsorbent for Cr (VI) ions. *Sci. Rep.* 11, 16598. <https://doi.org/10.1038/s41598-021-96145-6>.
- Eltaweil, A.S., Elgarhy, G.S., El-Subruiti, G.M., Omer, A.M., 2020. Carboxymethyl cellulose/carboxylated graphene oxide composite microbeads for efficient adsorption of cationic methylene blue dye. *Int. J. Biol. Macromol.* 154, 307–318. <https://doi.org/10.1016/j.ijbiomac.2020.03.122>.
- Ghaffari, S., Varshosaz, J., Haririan, I., Khoshayand, M.R., Azarmi, S., Gazori, T., 2012. Ciprofloxacin loaded alginate/chitosan and solid lipid nanoparticles, preparation, and characterization. *J. Dispers. Sci. Technol.* 33, 685–689. <https://doi.org/10.1080/01932691.2011.579831>.
- Ghorbani, F.M., Kaffashi, B., Shokrollahi, P., Seyedjafari, E., Ardeshiryajimi, A., 2015. PCL/chitosan/Zn-doped nHA electrospun nanocomposite scaffold promotes adipose derived stem cells adhesion and proliferation. *Carbohydr. Polym.* 118, 133–142. <https://doi.org/10.1016/j.carbpol.2014.10.071>.
- Hanna, D.H., Saad, G.R., 2019. Encapsulation of ciprofloxacin within modified xanthan gum-chitosan based hydrogel for drug delivery. *Bioorg. Chem.* 84, 115–124. <https://doi.org/10.1016/j.bioorg.2018.11.036>.
- Homayun, B., Lin, X., Choi, H.J., 2019. Challenges and recent progress in oral drug delivery systems for biopharmaceuticals. *Pharmaceutics* 11, 129–158. <https://doi.org/10.3390/pharmaceutics11030129>.
- Islan, G.A., Castro, G.R., 2014. Tailoring of alginate–gelatin microspheres properties for oral ciprofloxacin-controlled release against *Pseudomonas aeruginosa*. *Drug Deliv.* 21, 615–626. <https://doi.org/10.3109/10717544.2013.870257>.
- Islan, G.A., Mukherjee, A., Castro, G.R., 2015. Development of biopolymer nanocomposite for silver nanoparticles and ciprofloxacin controlled release. *Int. J. Biol. Macromol.* 72, 740–750. <https://doi.org/10.1016/j.ijbiomac.2014.09.020>.
- Khan, M.U.A., Yaqoob, Z., Ansari, M.N.M., Razak, S.I.A., Raza, M. A., Sajjad, A., Haider, S., Busra, F.M., 2021a. Chitosan/poly vinyl alcohol/graphene oxide based pH-responsive composite hydrogel films: drug release, anti-microbial and cell viability studies. *Polymers* 13, 3124–3143. <https://doi.org/10.3390/polym13183124>.
- Khan, Y.A., Ozaltin, K., Bernal-Ballen, A., Di Martino, A., 2021b. Chitosan-alginate hydrogels for simultaneous and sustained releases of ciprofloxacin, amoxicillin and vancomycin for combination therapy. *J. Drug Delivery Sci. Technol.* 61, 102126–102139. <https://doi.org/10.1016/j.jddst.2020.102126>.
- Kibungu, C., Kondiah, P.P., Kumar, P., Choonara, Y.E., 2021. Recent advances in chitosan and alginate-based hydrogels for wound healing application. *Front. Mater.* 8, 293–308. <https://doi.org/10.3389/fmats.2021.681960>.
- Kim, J., Cote, L.J., Huang, J., 2012. Two dimensional soft material: new faces of graphene oxide. *Acc. Chem. Res.* 45, 1356–1364. <https://doi.org/10.1021/ar300047s>.
- Kolanthai, E., Sindu, P.A., Khajuria, D.K., Veerla, S.C., Kuppuswamy, D., Catalani, L.H., Mahapatra, D.R., 2018. Graphene Oxide—A Tool for the Preparation of Chemically Crosslinking Free Alginate–Chitosan–Collagen Scaffolds for Bone Tissue Engineering. *ACS Appl. Mater. Interfaces* 10 (15), 12441–12452.
- Kyzioł, A., Mazgala, A., Michna, J., Regiel-Futyrka, A., Sebastian, V., 2017. Preparation and characterization of alginate/chitosan formulations for ciprofloxacin-controlled delivery. *J. Biomater. Appl.* 32, 162–174. <https://doi.org/10.1177/0885328217714352>.
- Lengyel, M., Kállai-Szabó, N., Antal, V., Laki, A.J., Antal, I., 2019. Microparticles, microspheres, and microcapsules for advanced drug delivery. *Sci. Pharm.* 87, 20–51. <https://doi.org/10.3390/scipharm87030020>.
- Li, C., Wang, J., Wang, Y., Gao, H., Wei, G., Huange, Y., Yu, H., Gan, Y., Wang, Y., Mei, L., Chen, H., Hu, H., Zhang, Z.Y., Jin, Y., 2019. Recent progress in drug delivery. *Acta Pharm. Sin. B* 9, 1145–1162. <https://doi.org/10.1016/j.apsb.2019.08.003>.
- Li, J., Jin, H., Razzak, M., Kim, E.J., Choi, S.S., 2022a. Crosslinker-free bovine serum albumin-loaded chitosan/alginate nanocomplex for pH-responsive bursting release of oral-administered protein. *Biotechnol. Bioprocess Eng.* 27, 40–50. <https://doi.org/10.1007/s12257-021-0243-6>.
- Li, S., Zhang, H., Chen, K., Jin, M., Vu, S.H., Jung, S., He, N., Zheng, Z., Lee, M.-S., 2022b. Application of chitosan/alginate nanoparticle in oral drug delivery systems: prospects and challenges. *Drug Deliv.* 29, 1142–1149. <https://doi.org/10.1080/10717544.2022.2058646>.
- Liu, J., Dong, J., Zhang, T., Peng, Q., 2018. Graphene-based nanomaterials and their potentials in advanced drug delivery and cancer therapy. *J. Control. Release* 286, 64–73. <https://doi.org/10.1016/j.jconrel.2018.07.034>.
- Maiti, S., Sen, K.K., 2017. Introductory chapter: drug delivery concepts. *Adv. Technol. Deliv. Therapeutics* 1–12. <https://doi.org/10.5772/65245>.
- Marei, N., Elwahy, A.H., Salah, T.A., El Sherif, Y., Abd El-Samie, E., 2019. Enhanced antibacterial activity of egyptian local insects' chitosan-based nanoparticles loaded with ciprofloxacin-HCl. *Int. J. Biol. Macromol.* 126, 262–272. <https://doi.org/10.1016/j.ijbiomac.2018.12.204>.
- Meng, N., Su, Y., Zhou, N., Zhang, M., Shao, M., Fan, Y., Zhu, H., Yuan, P., Chi, C., Xiao, Y., 2016. Carboxylated graphene oxide functionalized with β -cyclodextrin-engineering of a novel nanohybrid drug carrier. *Int. J. Biol. Macromol.* 93, 117–122. <https://doi.org/10.1016/j.ijbiomac.2016.08.051>.
- Mohy Eldin, M.S., Hashem, A.E., Tamer, T.M., Omer, A.M., Yossuf, M.E., Sabet, M.M., 2017. Development of cross linked chitosan/alginate polyelectrolyte proton exchanger membranes for fuel cell applications. *International Journal of Electrochemical Science* 12 (5), 3840–3858.
- Mohy Eldin, M.S., Omer, A.M., Wassel, M.A., Tamer, T.M., Abd Elmonem, M.S., Ibrahim, S.A., 2015. Novel smart pH sensitive chitosan grafted alginate hydrogel microcapsules for oral protein delivery: I. Preparation and characterization. *Int. J. Pharm. Pharm. Sci.* 7, 331–337.
- Olate-Moya, F., Palza, H., 2022. Effect of graphene oxide on the pH-responsive drug release from supramolecular hydrogels. *J. Appl. Polym. Sci.* 139, 51420–51420. <https://doi.org/10.1002/app.51420>.
- Omer, A.M., Sadik, W.A.A., El-Demerdash, A.G.M., Hassan, H.S., 2021a. Formulation of pH-sensitive aminated chitosan–gelatin crosslinked hydrogel for oral drug delivery. *J. Saudi Chem. Soc.* 25, 101384–101401. <https://doi.org/10.1016/j.jscs.2021.101384>.
- Omer, A.M., Abd El-Monaem, E.M., Eltaweil, A.S., 2022. Novel reusable amine-functionalized cellulose acetate beads impregnated aminated graphene oxide for adsorptive removal of hexavalent chromium ions. *International Journal of Biological Macromolecules* 208, 925–934.
- Omer, A.M., Ahmed, M.S., El-Subruiti, G.M., Khalifa, R.E., Eltaweil, A.S., 2021b. pH-Sensitive alginate/carboxymethyl chitosan/aminated chitosan microcapsules for efficient encapsulation and delivery of diclofenac sodium. *Pharmaceutics* 13, 338–356. <https://doi.org/10.3390/pharmaceutics13030338>.
- Omer, A.M., Tamer, T.M., Khalifa, R.E., Eltaweil, A.S., Agwa, M. M., Sabra, S., Abd-Elmonem, E.M.A., Mohy-Eldin, M.S., Ziora, Z.M., 2021c. Formulation and antibacterial activity evaluation of quaternized aminochitosan membrane for wound dressing applications. *Polymers* 13, 2428–2448. <https://doi.org/10.3390/polym13152428>.

- Omer, A.M., El-Monaem, E.M.A., El-Subruiti, G.M., El-Latif, M.A., Eltaweil, A.S., 2021d. Fabrication of easy separable and reusable MIL-125 (Ti)/MIL-53 (Fe) binary MOF/CNT/Alginate composite microbeads for tetracycline removal from water bodies. *Sci. Rep.* 11, 23818. <https://doi.org/10.1038/s41598-021-03428-z>.
- Omer, A.M., Ziora, Z.M., Tamer, T.M., Khalifa, R.E., Hassan, M.A., Mohy-Eldin, M.S., Blaskovich, M.A., 2021e. Formulation of quaternized aminated chitosan nanoparticles for efficient encapsulation and slow release of curcumin. *Molecules* 26, 449–463. <https://doi.org/10.3390/molecules26020449>.
- Poosmaeil, M., Asl, E.A., Namazi, H., 2021. Simple fabrication of biocompatible chitosan/graphene oxide microspheres for pH-controlled amoxicillin delivery. *Eur. Polym. J.* 159, 110706–110718. <https://doi.org/10.1016/j.eurpolymj.2021.110706>.
- Rafi, A.A., Mahkam, M., 2015. Preparation of magnetic pH-sensitive microcapsules with an alginate base as colon specific drug delivery systems through an entirely green route. *RSC Adv.* 5, 4628–4638. <https://doi.org/10.1039/C4RA15170D>.
- Ravindra, S., Varaprasad, K., Narayana, N., Vimala, K., Mohana, K., 2011. Biodegradable microspheres for controlled release of an antibiotic ciprofloxacin. *J. Polym. Environ.* 19, 413–418. <https://doi.org/10.1007/s10924-011-0290-8>.
- Rehman, N., Dilshad, M.R., Islam, A., Gull, N., Riaz, T., Khan, S.M., Khan, R.U., 2021. Novel graphene oxide loaded sodium alginate hydrogels cross-linked with tetraethyl orthosilicate for cephradine release analysis. *J. Drug Deliv. Sci. Technol.* 66, 102784–102794. <https://doi.org/10.1016/j.jddst.2021.102784>.
- Sahoo, S., Chakraborti, C.K., Mishra, S.C., 2011. Qualitative analysis of controlled release ciprofloxacin/carbopol 934 mucoadhesive suspension. *J. Adv. Pharm. Technol. Res.* 2, 195–204. <https://doi.org/10.4103/2231-4040.85541>.
- Sengupta, I., Kumar, S.S.S., Gupta, K., Chakraborty, S., 2021. In-vitro release study through novel graphene oxide aided alginate based pH-sensitive drug carrier for gastrointestinal tract. *Mater. Today Commun.* 26, 101737–101772. <https://doi.org/10.1016/j.mtcomm.2020.101737>.
- Srinatha, A., Pandit, J., Singh, S., 2008. Ionic cross-linked chitosan beads for extended release of ciprofloxacin: in vitro characterization. *Indian J. Pharm. Sci.* 70, 16–21. <https://doi.org/10.4103/0250-474X.40326>.
- Sun, L., Fugetsu, B., 2013. Effect of encapsulated graphene oxide on alginate-based bead adsorption to remove acridine orange from aqueous solutions. *ArXiv Preprint ArXiv:1307.0223,1-22*. <https://doi.org/10.1016/j.cej.2013.10.083>.
- Sun, X., Liu, C., Omer, A.M., Yang, L.Y., Ouyang, X.K., 2019a. Dual-layered pH-sensitive alginate/chitosan/kappa-carrageenan microbeads for colon-targeted release of 5-fluorouracil. *Int. J. Biol. Macromol.* 132, 487–494. <https://doi.org/10.1016/j.ijbiomac.2019.03.225>.
- Sun, X., Liu, C., Omer, A.M., Lu, W., Zhang, S., Jiang, X., Wu, H., Yu, D., Ouyang, X.K., 2019b. pH-Sensitive ZnO/carboxymethyl cellulose/chitosan bio-nanocomposite beads for colon-specific release of 5-fluorouracil. *Int. J. Biol. Macromol.* 128, 468–479. <https://doi.org/10.1016/j.ijbiomac.2019.01.140>.
- Sung, Y.K., Kim, S.W., 2020. Recent advances in polymeric drug delivery systems. *Biomater. Res.* 24, 1–12. <https://doi.org/10.1186/s40824-020-00190-7>.
- Taher, M.A., Omer, A.M., Hamed, A.M., Ali, A.M., Tamer, T.M., Mohy Eldin, M.S., 2019. Development of smart alginate/chitosan grafted microcapsules for colon site-specific drug delivery. *Egypt. J. Chem.* 62, 1037–1045. <https://doi.org/10.21608/EJCHEM.2019.6716.1562>.
- Tahtat, D., Mahlous, M., Benamer, S., Khodja, A.N., Oussedik-Oumehdi, H., Laraba-Djebari, F., 2013. Oral delivery of insulin from alginate/chitosan crosslinked by glutaraldehyde. *Int. J. Biol. Macromol.* 58, 160–168. <https://doi.org/10.1016/j.ijbiomac.2013.03.064>.
- Tamer, T.M., Abou-Taleb, W.M., Roston, G.D., Mohyeldin, M.S., Omer, A.M., Khalifa, R.E., Hafez, A.M., 2018. Formation of zinc oxide nanoparticles using alginate as a template for purification of wastewater. *Environmental Nanotechnology, Monitoring and Management* 10, 112–121.
- Tamer, T.M., Omer, A.M., Hassan, M.A., Hassan, M.E., Sabet, M.M., Mohy Eldin, M.S., 2015. Development of thermo-sensitive poly N-isopropyl acrylamide grafted chitosan derivatives. *J. Appl. Pharm. Sci.* 5, 001–006. <https://doi.org/10.7324/JAPS.2015.510.S1>.
- Ubaid, M., Murtaza, G., 2018. In vitro evaluation of genipin-crosslinked Na-alginate/chitosan hydrogel films for delivery of metformin: Effect of chitosan molecular weight. *Curr. Drug Deliv.* 15, 1146–1158. <https://doi.org/10.2174/1567201815666180409102459>.
- Varma, M.V., Kaushal, A.M., Garg, A., Garg, S., 2004. Factors affecting mechanism and kinetics of drug release from matrix-based oral controlled drug delivery systems. *Am. J. Drug Deliv.* 2, 43–57.
- Vinken, M., Rogiers, V., 2015. *Protocols in in-vitro hepatocyte research*, Springer. <https://doi.org/10.1007/978-1-4939-2074-7>.
- Zhang, H., Pang, X., Qi, Y., 2015. pH-Sensitive graphene oxide/sodium alginate/polyacrylamide nanocomposite semi-IPN hydrogel with improved mechanical strength. *RSC Adv.* 5, 89083–89091. <https://doi.org/10.1039/C5RA19637J>.
- Zhang, M., Liang, J., Yang, Y., Liang, H., Jia, H., Li, D., 2020. Current trends of targeted drug delivery for oral cancer therapy. *Front. Bioeng. Biotechnol.* 8, 1417–1428. <https://doi.org/10.3389/fbioe.2020.618931>.
- Zheng, H., Yang, J., Han, S., 2016. The synthesis and characteristics of sodium alginate/graphene oxide composite films crosslinked with multivalent cations. *J. Appl. Polym. Sci.* 133, 43616–43623. <https://doi.org/10.1002/app.43616>.